SEMARAK ILMU PUBLISHING

Journal of Advanced Research in Fluid Mechanics and Thermal Sciences

Journal homepage:
https://semarakilmu.com.my/journals/index.php/fluid_mechanics_thermal_sciences/index
ISSN: 2289-7879

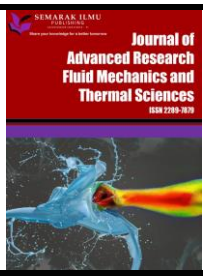

Effect of the Catalyst Shapes and the Packed Bed Structure on the Efficiency of Steam Methane Reforming

Ravil Mustafin[1,*], Igor Karpilov[1]

[1] Department of Industrial Engineering, Faculty of Thermal Engineering, Samara State Technical University, Samara, Russia

ARTICLE INFO

Article history:
Received 27 November 2022
Received in revised form 12 February 2023
Accepted 20 February 2023
Available online 13 March 2023

Keywords:
Steam methane reforming; hydrogen; reformer design

ABSTRACT

One of the promising technologies for on-board hydrogen production is methane steam reforming in reactor with packed bed. The study of the effect of various catalytic packing arrangements on the steam methane reforming process is of considerable interest. The present article analyses the influence of catalyst shapes and packing arrangement on steam methane reforming reactions efficiency. The reformer tube contains several packings with a changing relative position; additionally, two forms of catalysts, a ball and a cylinder, are also used. The pressure drop depending on the packing location, methane conversion and hydrogen yield were analysed. It was found that the packing arrangement with spacing allows better distribution of the supplied heat. Due to the distance between the packing sections flow becomes more turbulent after each section, which intensifies the heat transfer and mixing of the mixture. The highest hydrogen yield is observed on catalytic packings located at a distance of 40 mm from each other and consisting of cylindrical catalysts. The most uniform pressure drop occurs at a packing arrangement without spacing. The increase in methane conversion observed with the increment in spacing distance, but the difference is insignificant. Therefore, the arrangement of catalysts with spacing can be used for the improvement of steam methane reforming process.

1. Introduction

Currently, there is a global trend of switching from fossil fuels to renewable energy sources. That process is greatly influenced by policies aimed on climate change mitigation and the big breakthrough in the field of alternative energy. However, it is impossible to solve all energy problems at once by simply switching from one energy source to another, this issue requires a comprehensive approach. There are many industries where the transition from fossil fuels is of great difficulty as this will reduce their productivity [1-2]. Examples of such industrial areas are metallurgy, glass production, various electric and thermal power plants. Many countries use different energy saving technologies as it helps to reduce fuel consumption and emissions of harmful substances into the atmosphere [3-4].

* *Corresponding author.*
E-mail address: ravil-bk211@mail.ru

https://doi.org/10.37934/arfmts.104.1.124140

One of the promising energy saving technologies is the use of secondary energy sources, for example, flue gases released after the combustion process. There are many ways of flue gas industrial use, for example, in article [5] authors suggest using the heat of flue gases to heat the water, which reduces the boiler fuel consumption. Another method is thermochemical regeneration of the heat of exhaust flue gases due to endothermic reactions. The heat of flue gases is used for the heat supply for reforming reactions and the reaction products (with high hydrogen content) may be combusted in the fuel consuming equipment or stored. Thus, the heat of flue gases is stored as chemical energy of the transformed fuel. This method allows not only to sensibly use the flue gas heat but also to improve the facility energy efficiency [6].

The latest published articles are focused primarily on steam methane reforming process optimization. The optimal values of temperature, velocity, pressure, steam to methane ratio and oxidizer composition are of great interest. Pashchenko [7] performed the experimental and numerical analysis of steam methane reforming reactions in a microchannel reformer. He determined, that with the increasing Reynolds number the hydrogen yield is decreasing. Also, the methane conversion rate is practically three times higher if reactor temperature rises from 800K to 1000K.

The industrial schemes with the implementation of thermochemical regeneration were assessed by Popov *et al.,* [8]. The authors compared the industrial process scheme in a glass furnace to an upgraded version with thermochemical recuperation and concluded that efficiency could be higher in a range of 10-25% without affecting other parameters of the process.

In the aforementioned articles, the steam methane reforming process was studied by thermochemical analysis in Aspen Hysys and Mathcad. These programs give valuable information on the reaction products but they cannot be used to investigate the distribution of the parameters inside the reactor. A better understanding of this phenomenon is crucial to further reactor performance enhancement. Computer modelling is widely used to simulate species and temperature distribution, pressure drop and other parameters [9-11].

In [9-14] the authors describe a method of thermochemical regeneration due to steam-methane reforming. The reaction of methane conversion occurs in the reactor near catalyst's surface. Main reaction product is a synthetic fuel with very high hydrogen concentration, which has a rather high calorific value. Karthik and the authors in their article [14] investigated the influence of catalyst shapes on changes in pressure drop and the reaction characteristics. Their study showed, that various forms and quantities of catalysts have considerable influence on the course of endothermic reactions.

Therefore, the study of the catalyst packing location influence on steam methane reforming characteristics is of great interest. The aim of the work is to study the influence of different catalytic packing arrangements on the thermochemical reactor performance. One of the reactor key parameters is methane conversion. So, the dependence of methane conversion on the spacing distance between catalyst packing sections is studied.

2. Methodology

In this article, two forms of the catalyst were considered: the cylindrical shape and the ball shape. Three catalyst packings consisting of five elements each were used. The effect of the different distance between packing sections on the reaction and flow performance was studied. Additional distance between the packing sections provides additional mixing of the reaction mixture, which may lead to higher methane conversion. The steam-methane mixture flows through that arrangement of catalysts and due to narrow channels between catalyst and reformer wall flow becomes turbulent,

which in turn leads to a change in the pressure drop and hydrogen yield. The commercially available Ni-based catalyst was chosen for this study due to its low cost, widespread use and high efficiency. Figure 1. shows the schematic diagram of the reactor used in present work.

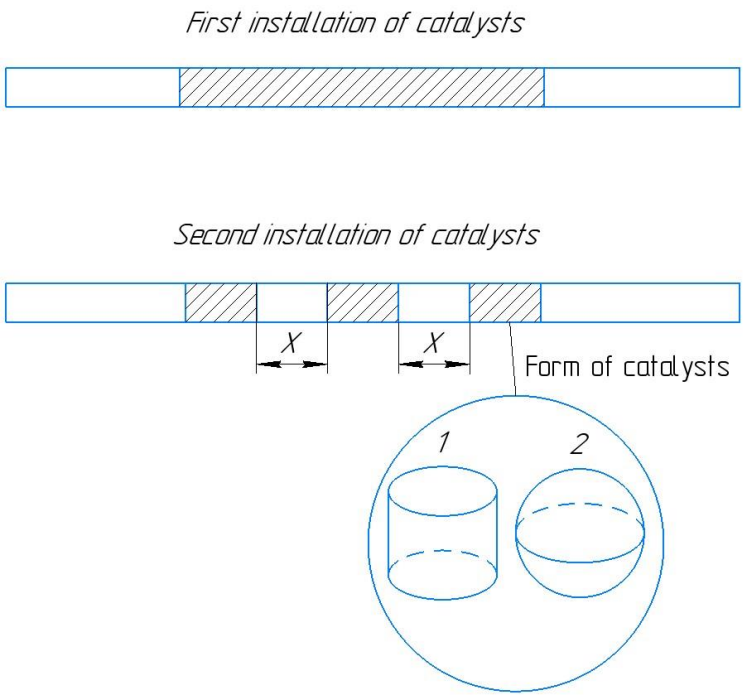

Fig. 1. Schematic diagram of the shapes and location of the catalyst packing

One of the most effective ways to study these problems is CFD modeling, which allows to visually assess the key parameters of the ongoing processes. In the present article the software package Ansys Fluent is utilized. Ansys Fluent uses finite volumes method (FVM) to solve the partial differential equations.

2.1 Model Geometry

Model geometry is a tube filled with catalysts. The diameter of the tube is 13 mm and the length is 500 mm. The catalysts are presented in the form of cylinders with a diameter of 10 mm and a height of 10 mm and balls with a diameter of 10 mm. The packed bed contains 3 separate sections with 5 randomly arranged catalysts in each section. The packing sections are located at a distance of X = 0, 20, 40, 80 mm from each other. The tube wall is also divided into separate sections along the packed bed region. The wall partition is used to define the heat flow on the tube surface. The details will be discussed below in the boundary conditions section. Figure 2 shows the model geometry with a packed bed consisting of cylinders, created in Ansys Fluent.

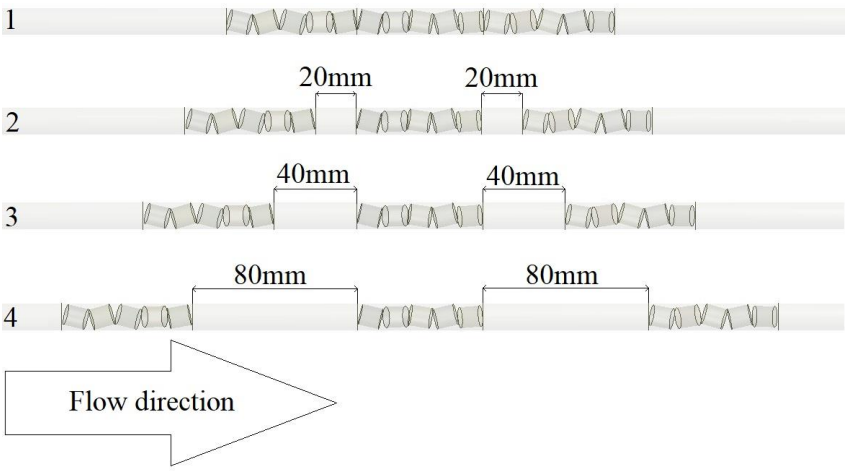

Fig. 2. Reactor geometry with cylindrical shape catalysts

Figure 3 shows the model geometry with a packed bed consisting of balls, constructed in Ansys Fluent.

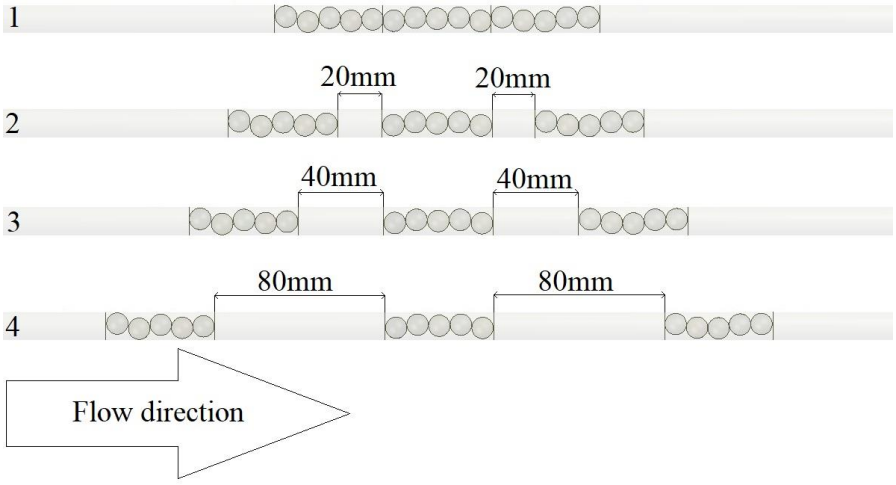

Fig. 3. Reactor geometry with spherical shape catalysts

2.2 Mesh

Ansys Fluent solves the model equations by the finite-element approach. The computational domain was divided into tetrahedral elements to obtain the computational mesh. The choice of tetrahedral mesh is motivated by rather complex geometry.

The model geometry was cut into finite elements, resulting in a numerical mesh. To obtain plausible results, a fine grid with a high number of elements was created. It is also important to refine the mesh in the boundary layer, i.e., near the catalysts. Triangular pyramids were chosen as grid elements since these elements are the simplest in the field of CFD modeling of such problems. To refine the mesh near the catalyst's surface, the Sizing procedure was used. As a result, a mesh with a total number of elements equal to about 3 million was obtained. In Figure 4 and Figure 5 the numerical mesh for catalysts with cylindrical and spherical forms are presented.

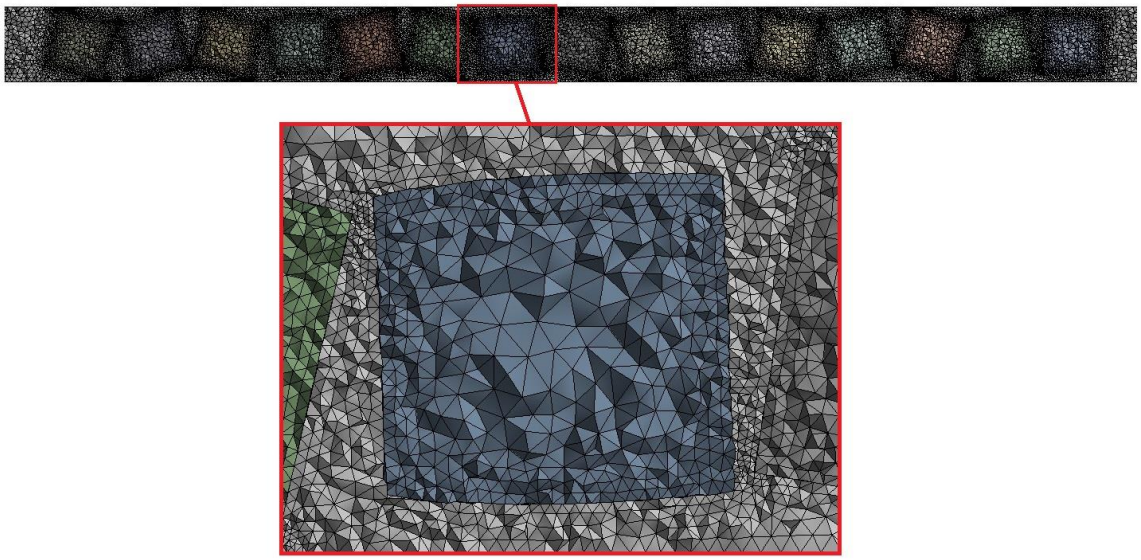

Fig. 4. Mesh for geometry with cylindrical catalysts

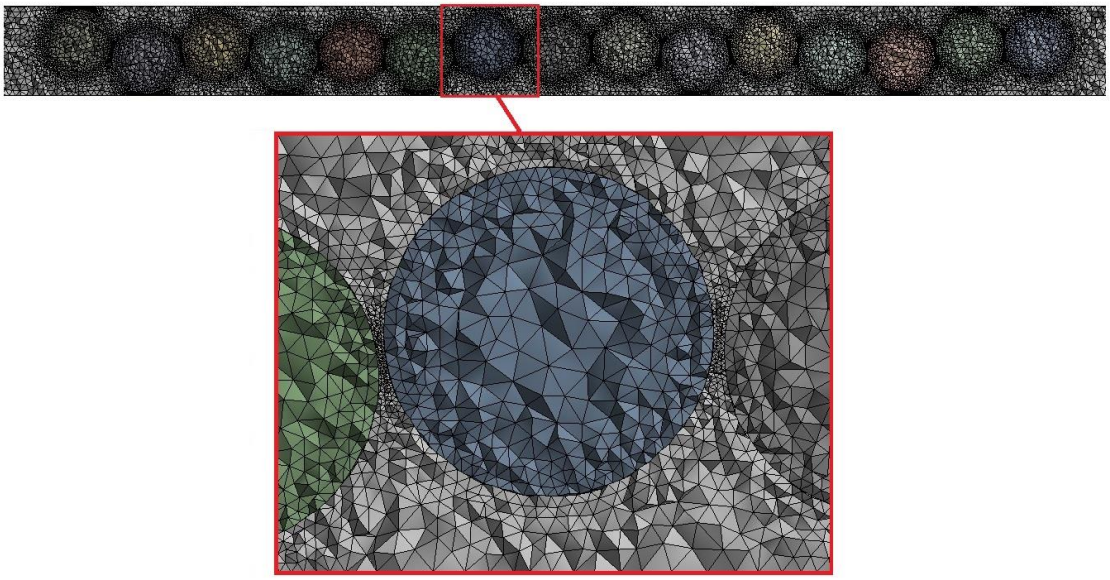

Fig. 5. Mesh for geometry with spherical catalysts

2.3 Governing Equation

The flow of liquid. To solve single-phase unsteady flows, Ansys Fluent uses the Reynolds-averaged equations of mass and momentum conservation

$$\frac{\partial \rho}{\partial t} + \nabla \cdot (\rho \bar{U}) = 0 \tag{1}$$

$$\frac{\partial (\rho \bar{U})}{\partial t} + \nabla \cdot (\rho \bar{U} \bar{U}) = -\nabla P - \nabla \cdot (\bar{\bar{\tau}} + \bar{\bar{\tau}}_t) + \rho \bar{g} + S_P \tag{2}$$

where $\bar{U}$ and P are mean velocity and pressure, $\bar{\bar{\tau}}$ and $\bar{\bar{\tau}}_t$ are viscous and turbulent stress tensors, $\rho \bar{g}$ is the gravitational body force, S_P is the momentum sink due to the porous media. The viscous stress tensor $\bar{\bar{\tau}}$ for a Newtonian fluid is given by

$$\bar{\bar{\tau}} = -\mu(\nabla\bar{U} + (\nabla\bar{U})^T) - \left(\frac{2}{3}\mu - k\right)(\nabla\cdot\bar{U})\bar{\bar{\delta}} \tag{3}$$

where l is the molecular viscosity and the second term on the right-hand side of the equation is the effect of volume dilation. The Reynolds stresses are modelled using the Boussinesq hypothesis as follows

$$\bar{\bar{\tau}}_t = \mu_t(\nabla\bar{U} + (\nabla\bar{U})^T) - \frac{2}{3}(\mu_t(\nabla\cdot\bar{U}) + \rho k)\bar{\bar{\delta}} \tag{4}$$

where μ_t ,is the turbulent viscosity. Based on literature information [15], the shear-stress (SST) $k-\omega$ model which computes μ_t in terms of turbulent kinetic energy (k) and turbulence eddy frequency (ω) was used in this work. The SST $k-\omega$ model [16] has the ability to solve the flow variables all the way to the wall without using wall functions. However, the model needs a fine mesh $(y^+ \leq 1)$ to resolve the boundary layer which has been taken care of in the present work. The description of the equations solved in this model are described in the reference guide [17].

A porous media approach was used to model flow, reaction, and diffusion through particle (solid domain). A large momentum source (S_p in Eq. (2)) as defined in Eq. (5) was used for the solid domain which suppressed the convective flux across the fluid-solid interface. Due to this, only the diffusion dominated inside the solid particles.

$$S_p = -\frac{\mu}{K_{\text{perm}}}\bar{U} - K_{\text{loss}}\frac{\rho}{2}|\bar{U}|\bar{U} \tag{5}$$

where K_{perm} is the permeability and K_{loss} is the quadratic loss coefficient. The first and second term in Eq. (5) represents the viscous and inertial losses, respectively.

Energy Transport. The temperature distribution in turbulent flow was simulated by solving the enthalpy equation with negligible effect of viscous dissipation for low mach number (M) flows as

$$\frac{\partial(\rho h)}{\partial t} + \nabla\cdot(\rho\bar{U}h) = \nabla\cdot\left((\lambda+\lambda_t)\nabla T\right) + \nabla\cdot\left(\sum_{i=1}^{n} h_i\rho\left(D_i + D_{t,i}\right)\nabla Y_i\right) + S_h \tag{6}$$

where h is the mean (Reynolds averaged) static enthalpy (and not the total enthalpy) and was calculated as $h = \sum h_i Y_i$, λ is the thermal conductivity, λ_t is the thermal conductivity due to turbulent transport, D_i is the molecular diffusivity of i^{th} species in the multicomponent mixture, $D_{t,i}$ is the mass diffusivity of i^{th} species due to turbulent transport, Y_i is the mass fraction of i^{th} species and S_h is the heat source due to chemical reactions. In Eq. (6), h_i is the enthalpy of i^{th} species defined as

$$h_i = \int_{T_{\text{ref}}}^{T} C_{p,i}(T)dT \tag{7}$$

λ_t was calculated using μ_t and the turbulent Prandtl number (Pr_t) as

$$\lambda_t = \frac{\hat{C}_p\mu_t}{Pr_t} \tag{8}$$

where $\hat{C}_p$ is the specific heat capacity and the value of Pr_t was 0.9. The heat transport inside the catalyst was simulated by solving Eq. (6) in which an effective thermal conductivity of solid (λ_{eff}) was used in place of λ. The heat release or intake by the chemical reactions inside the catalyst particle can be defined as

$$S_h = \rho_s \sum_{j=1}^{m} r_j\left(-\Delta H_j\right) \quad (9)$$

where ρ_s is the particle density, r_j and ΔH_j are the reaction rate and the heat of reaction for reaction j, respectively.

Species Transport. For diffusion and chemical reaction studies, the MSR reaction as given below were considered [23]

$$CH_4 + H_2O \leftrightarrow CO + 3H_2;\ \Delta H_1 = 206.1\ \text{kJ/mol} \quad (10)$$

$$CO + H_2O \leftrightarrow CO_2 + H_2;\ \Delta H_2 = -41.15\ \text{kJ/mol} \quad (11)$$

$$CH_4 + 2H_2O \leftrightarrow CO_2 + 4H_2;\ \Delta H_3 = 165.0\ \text{kJ/mol} \quad (12)$$

The species mass fraction distribution in the gas phase was simulated by solving species transport equation for $n-1$ species as

$$\frac{\partial(\rho Y_i)}{\partial t} + \nabla\cdot(\rho\bar{U}Y_i) = \nabla\cdot\left(\rho\left(D_i + D_{t,i}\right)\nabla Y_i\right) + S_i \quad (13)$$

where D_i and $D_{t,i}$ are the molecular and turbulent diffusivities of the i^{th} species in the multicomponent mixture, respectively and S_i is the rate of species formation or consumption by chemical reaction for species i. D_i was modeled using the Wilke correlation [18] and the corresponding binary diffusion coefficient using the Fuller *et al.,* correlation [19]. $D_{t,i}$ was computed from lt and the turbulent Schmidt number (Sc_t) as

$$D_{t,i} = \frac{\mu_t}{Sc_{t,i}} \quad (14)$$

where ρ is the density and Sc_t was taken to be 0.9. The species mass fraction distribution in particles was simulated by solving Eq. (13) in which an effective diffusivity ($D_{\text{eff},i}$) was used in place of D_i. $D_{\text{eff},i}$ was defined using the particle porosity (ε) and tortuosity (τ) values of 0.44 and 3.54, respectively [4] as

$$D_{\text{eff}} = \frac{\in_s}{\tau_s} D_i \quad (15)$$

The species formation or consumption by the chemical reaction inside the catalyst particle was accounted through species source or sink terms as

$$S_i = \rho_s \sum_{j=1}^{n} (\alpha_{ij} r_j) M_i \quad (16)$$

where ρ_s is the particle density, α_{ij} represents the stoichiometric coefficient of component i in the reaction j, and M_i is the molecular weight of species i. The species and heat source term in the particle were defined based on the Hou and Hughes [20] kinetic model for MSR over a $Ni/\alpha Al_2O_3$ catalyst.

2.5 Boundary Conditions and Model Validation

The calculation was carried out in the Ansys Fluent 2019 R2 software package, on 16 Xeon E5-2640 v4 processors. The operating conditions were as follows: atmospheric pressure, temperature 293K. The catalysts were set as a porous region with porosity of 0.44. A mixture of CH_4 + H_2O with a ratio of 1/2 was fed to the tube inlet, the mixture inlet temperature was 1100K and the speed was 0.25 m/s. The reaction kinetics was set by a custom function written in C language. As a reaction kinetic basis on the commercial Ni-based catalysts the data from Xu and Froment [22] was implemented. The following assumptions were made

i. calculations were performed in steady state regime;
ii. no energy flux due to a mass concentration gradient;
iii. no additional surface oxidation reactions (metal oxidation reactions);
iv. fresh catalyst is modeled (no carbon deposition on the catalyst surface).

Verification of the custom function and numerical approach was carried out in the article [21] by our research team, so verification was not carried out in the present work. The tube wall was divided into sections; the length of each section was equal to the length of the packed bed section. This was necessary to supply only the packing section with heat. A heat flux of 400 W/m^2 was supplied to wall 2, heat flux of 600 W/m^2 was supplied to wall 3. As the mixture flowed through the first packing layer it rapidly cooled down due to the occurring endothermic reactions. Therefore, it is necessary to supply heat to the other packing layers. Also, for comparison, the calculation was carried out without heat supply to the walls. In Fig. 6. the diagram of heat supply to the packing sections is shown.

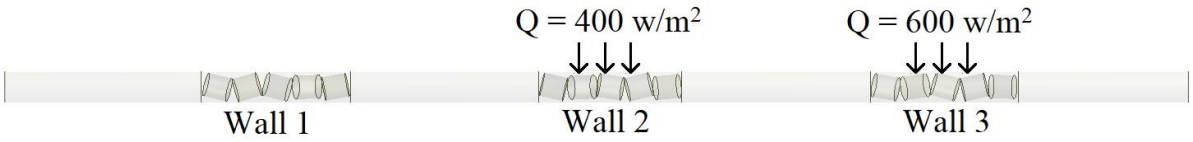

Fig. 6. Scheme of wall heat flux setting

3. Results

During the reactions without heat supply, the results presented in Figure 7 to Figure 10 were obtained. The conversion of methane was not affected by the location of the packed bed sections.

Figure 7 shows the contour of hydrogen mass fraction on cylindrical catalysts without heat supply to the reactor walls. It can be seen that the hydrogen yield does not change depending on the location

of the packed bed sections. Observed effect is due to the rather low temperatures after the first packing section as more heat is required to obtain high reaction rates.

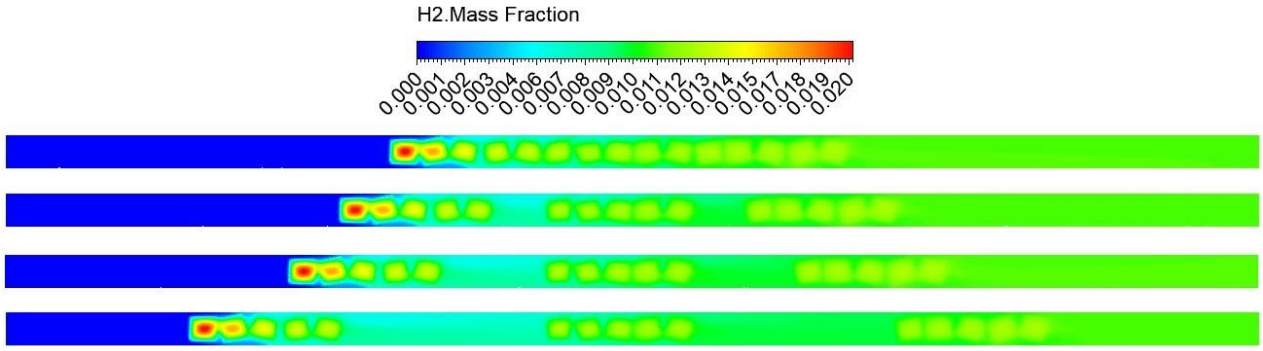

Fig. 7. The contour of hydrogen mass fraction for catalysts with cylindrical shape without wall heat flux

Figure 8 shows the contour of methane mass fraction on cylindrical catalysts without additional heat flux. It can be observed that, regardless of the packing sections location, the amount of converted methane remains unchanged. That strongly correlates with hydrogen fraction distribution as methane is reactant and hydrogen is reaction product. So, the fraction distribution should be practically identical, but reversed.

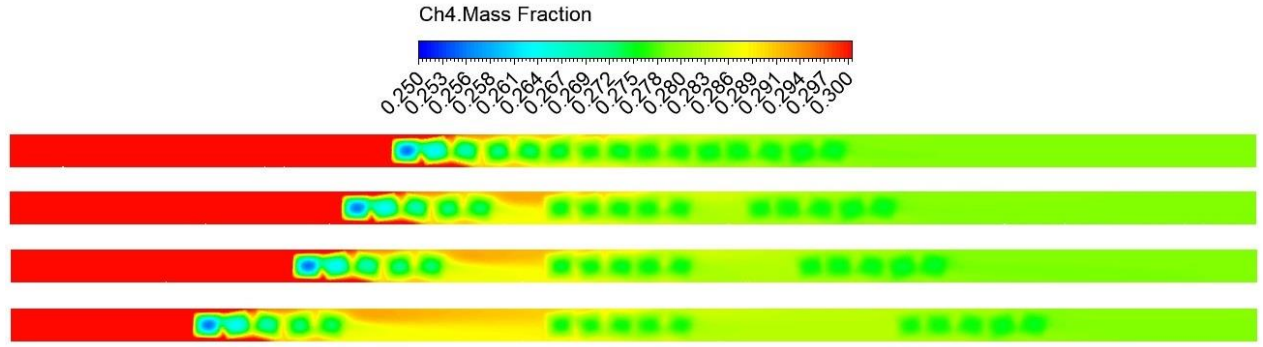

Fig. 8. The contour of methane mass fraction for catalysts with cylindrical shape without wall heat flux

Figure 9 shows the contour of hydrogen mass fraction on spherical catalysts without heat supply. It can be seen that the hydrogen yield does not change depending on the catalyst packing arrangement. The observed behavior is similar to the results obtained for cylindrical catalyst. The reasons are deemed similar as well.

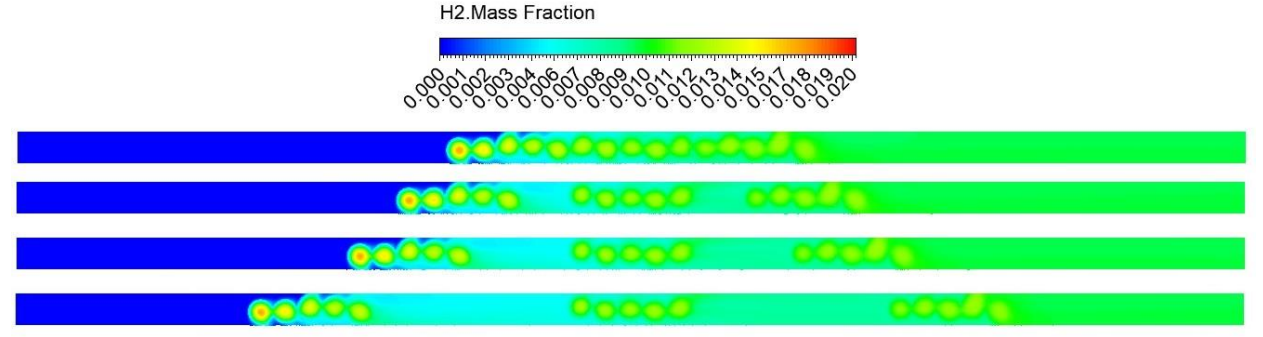

Fig. 9. The contour of hydrogen mass fraction for catalysts with spherical shape without wall heat flux

Figure 10 shows the contour of methane mass fraction on spherical catalysts without heat supply. It can be seen that catalyst packing configuration has no effect on the amount of converted methane. Methane conversion on cylindrical catalyst is more active than on spherical ones for the first packing section. That effect was also observed by Karhik [14].

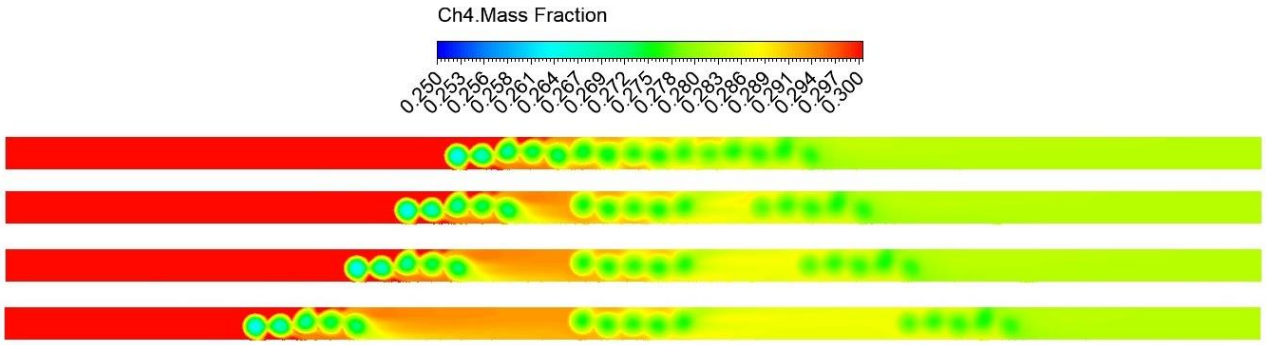

Fig. 10. The contour of methane mass fraction for catalysts with spherical shape without wall heat flux

Figure 11 and Figure 12 show the temperature contours for various shapes and locations of the packing sections. It can be seen that the temperature practically did not change when the spacing between sections was increased. Particle shape also has negligible effect on the temperature distribution as the main driving factor is heat of the endothermic reaction. Additional heat flux to the reactor wall could provide more heat for the reaction and make the particle shape influence more pronounced.

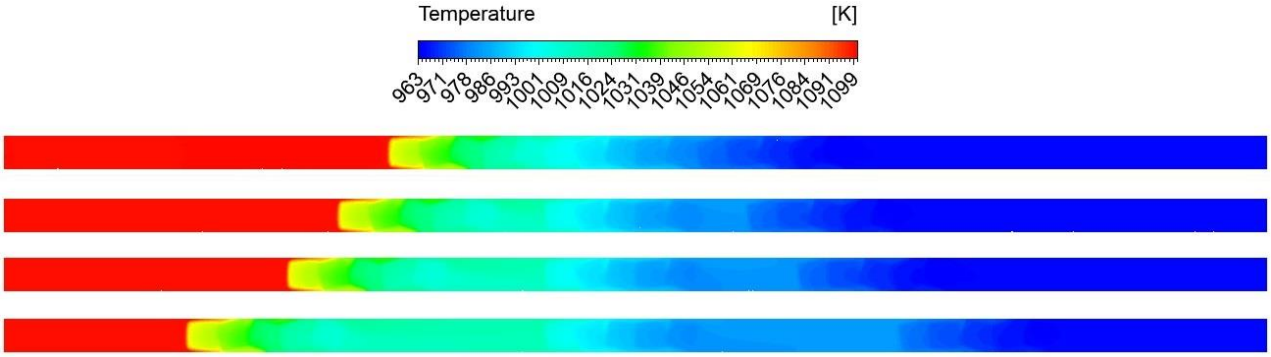

Fig. 11. Temperature contour for catalysts with cylindrical shape without wall heat flux

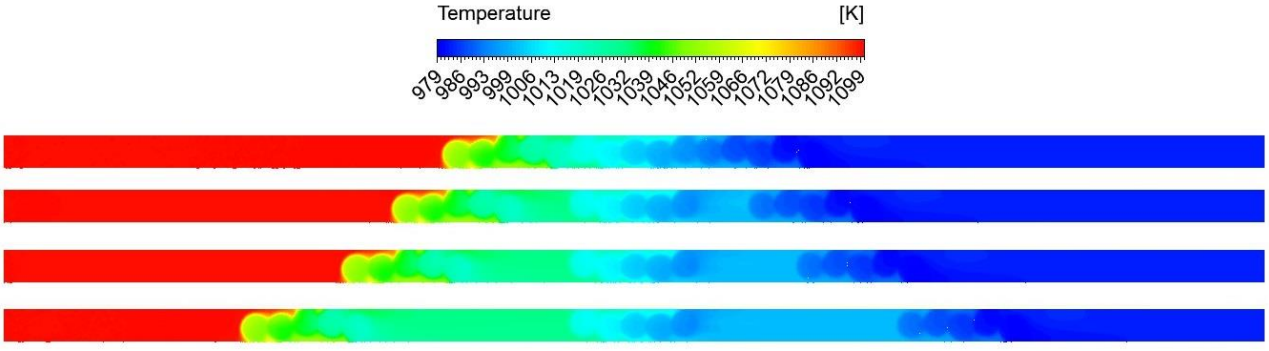

Fig. 12. Temperature contour for catalysts with spherical shape without wall heat flux

Figure 13 shows the velocity vector field for cylindrical catalysts. It can be seen that a turbulence of the flow occurs behind the cylindrical catalysts. It is stronger than for spherical catalysts due to the

better streamlining of the latter. Figure 14 shows the velocity vector field for spherical catalysts. It can be seen that there is less turbulence of the flow behind spherical catalysts than behind cylindrical catalysts. After each section vortices occur, which contribute to the steam methane reforming intensification due to changes in speed and an increase in temperature.

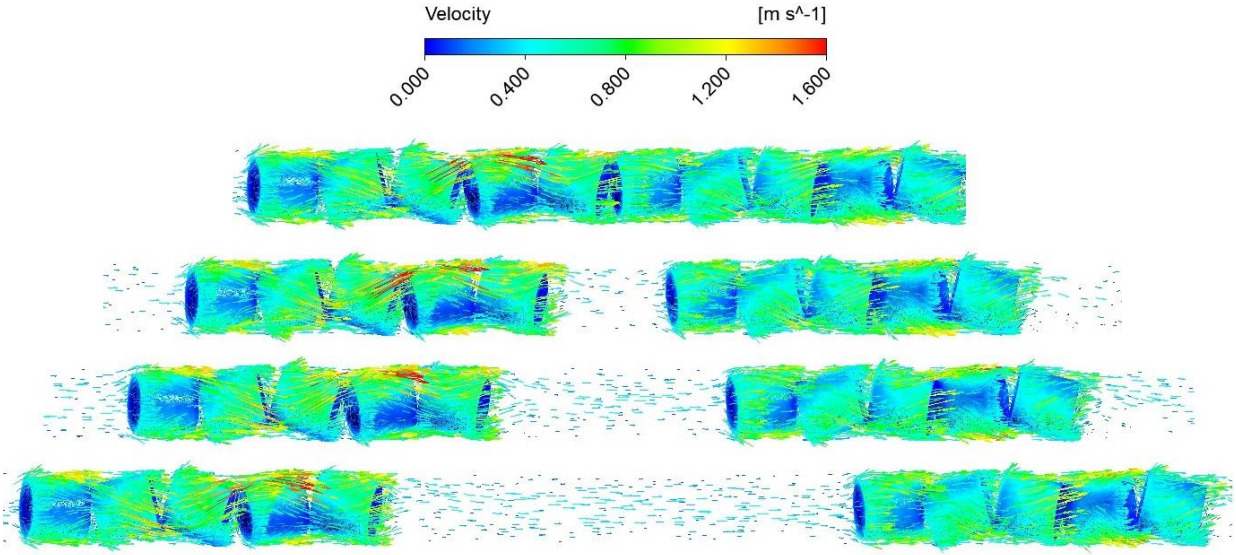

Fig. 13. Velocity contour for catalysts with cylindrical shape

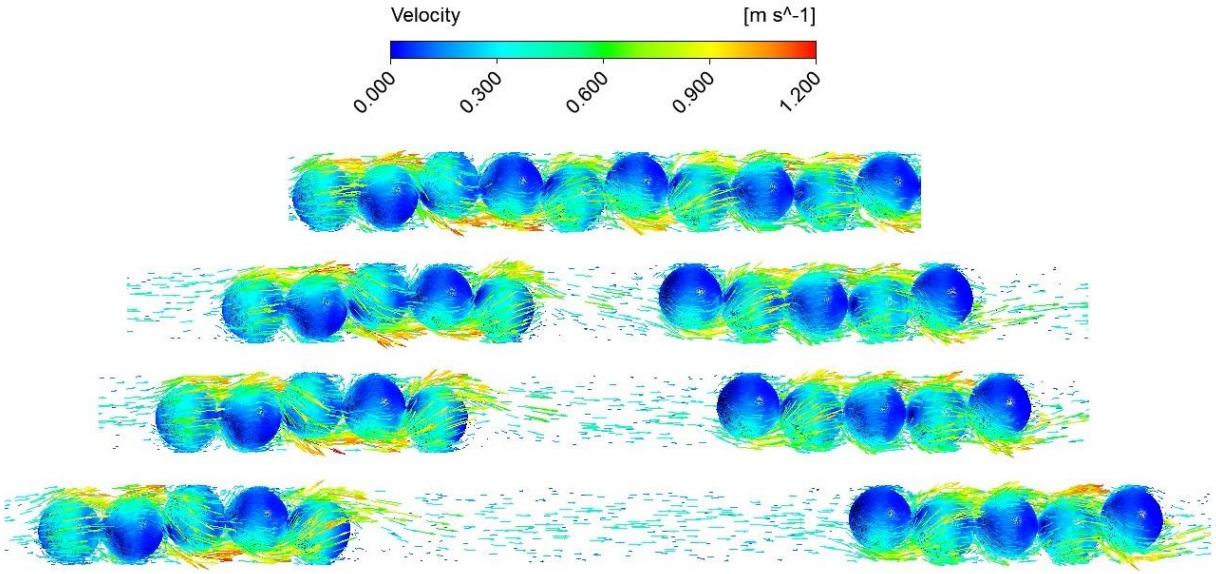

Fig. 14. Velocity contour for catalysts with spherical shape

The results of steam methane reforming with heat supply to the reformer walls are shown in Figure 15 - 18. It is clear that on the cylindrical catalysts, when the distance between the packing sections increases, more hydrogen is released. When the distance between the packings is equal to 40 mm, the highest hydrogen yield is observed, while at a distance of 80 mm the amount of hydrogen decreases, therefore, the best choice of the distance between the packing layers is the distance between 40 mm and 80 mm. The reaction rate intensification on the catalysts with spherical shape is not observed. It can be seen that, regardless of catalyst packing arrangement, the amount of converted methane remains unchanged. A possible reason is the good shape streamlining, which

does not contribute to the occurrence of large vortices. For all cases considered spherical catalysts showed worse performance than cylindrical ones from the methane conversion rate and hydrogen yield perspective. The finding is in good agreement with the literature [14].

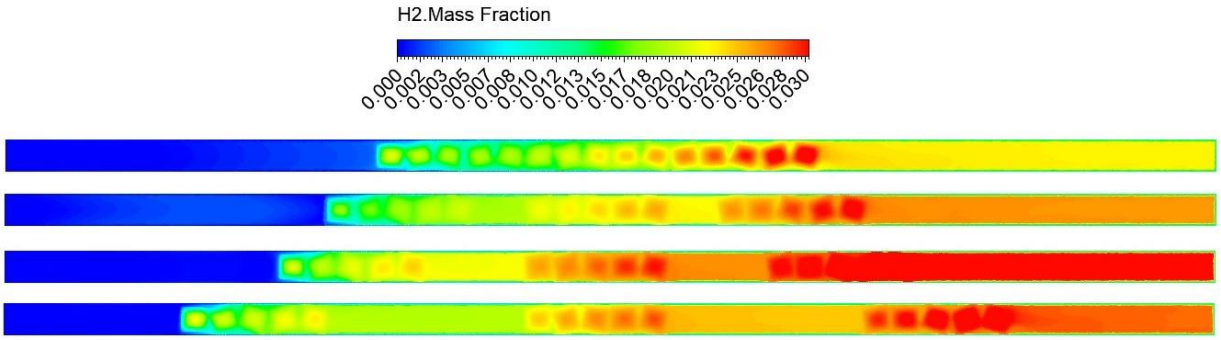

Fig. 15. The contour of hydrogen mass fraction for catalysts with cylindrical shape with wall heat flux

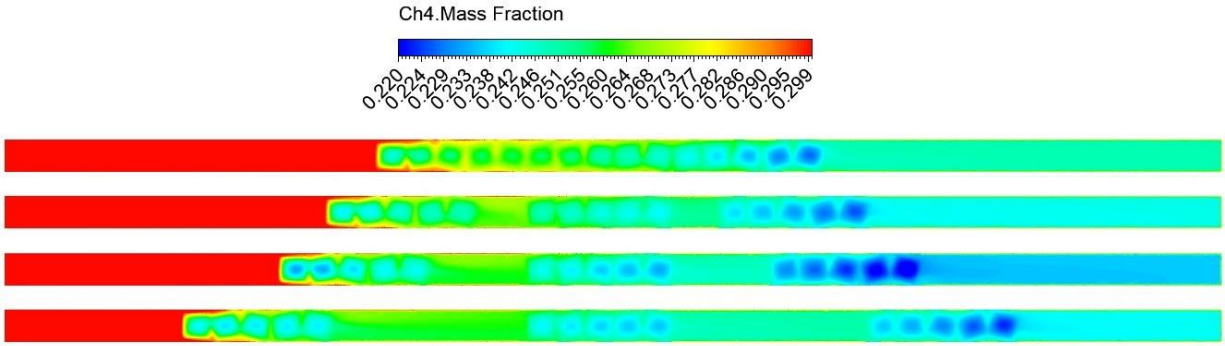

Fig. 16. The contour of methane mass fraction for catalysts with cylindrical shape with wall heat flux

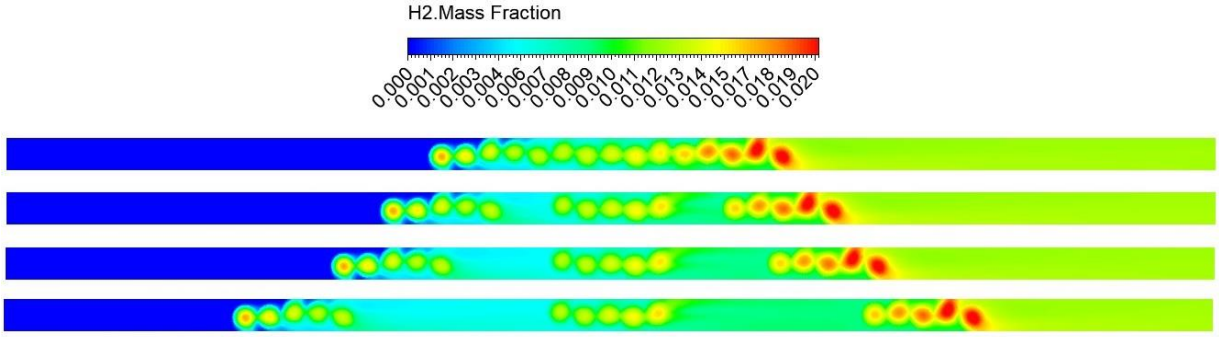

Fig. 17. The contour of hydrogen mass fraction for catalysts with spherical shape with wall heat flux

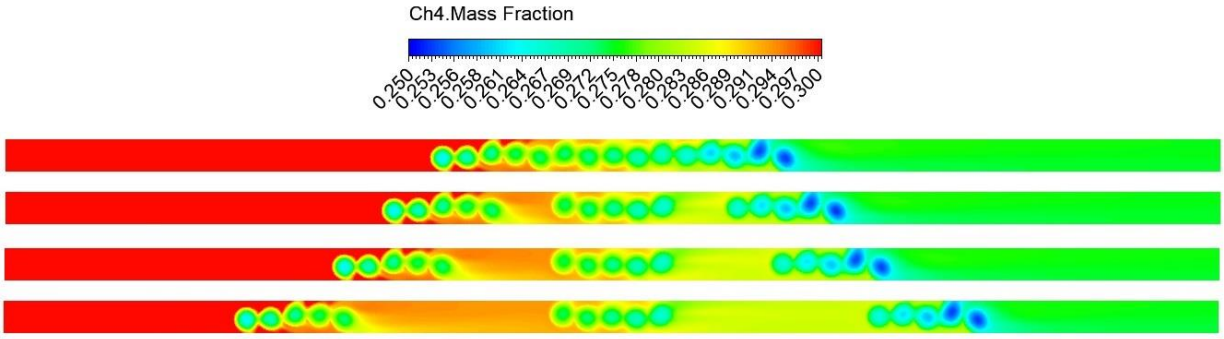

Fig. 18. The contour of methane mass fraction for catalysts with spherical shape with wall heat flux

Figure 19 and Figure 20 show the temperature contours for different shapes and locations of packing sections are presented. The contour with cylindrical shaped catalysts (Figure 19) shows that the temperature to which the catalysts are cooled is different and the greatest cooling occurs at a distance of 40 mm between the catalysts. On the spherical shape of the catalysts, the temperature variance is the same.

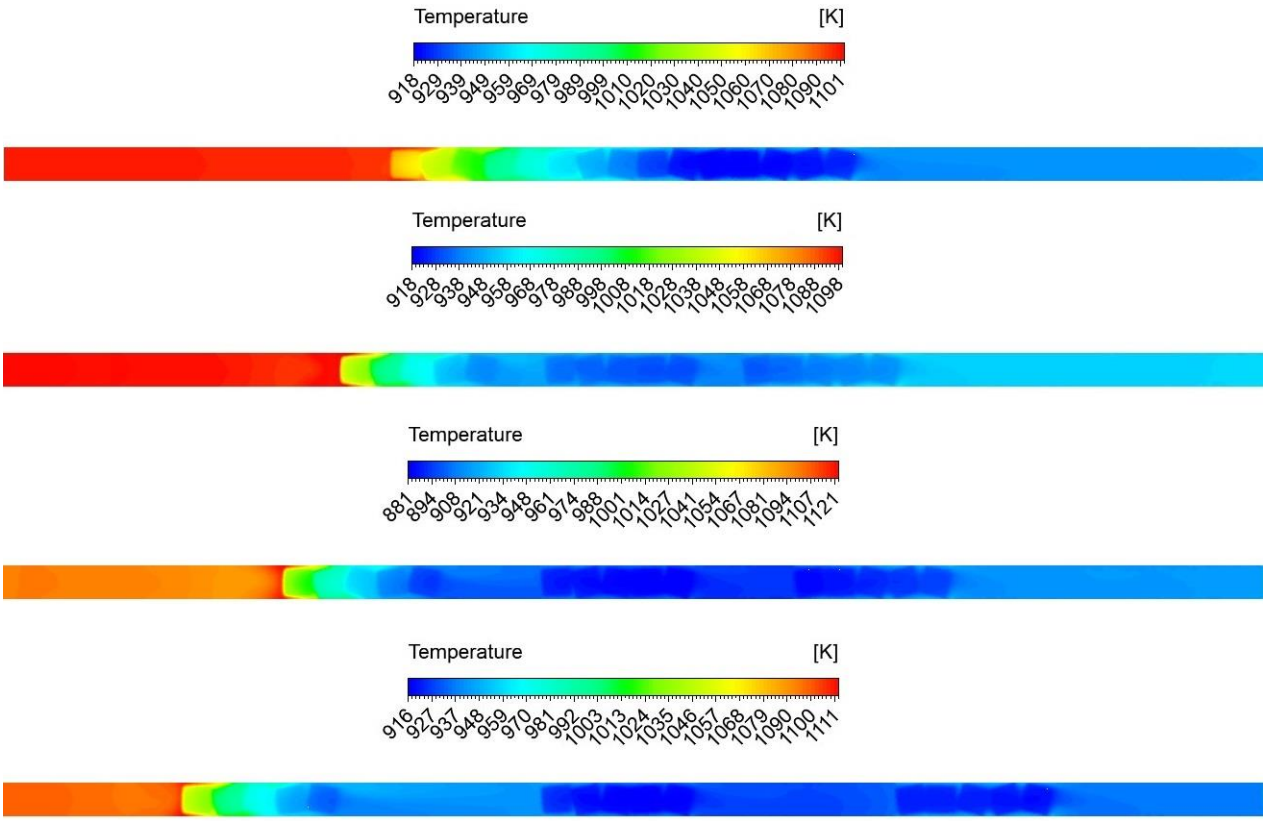

Fig. 19. Temperature contour for catalysts with cylindrical shape with wall heat flux

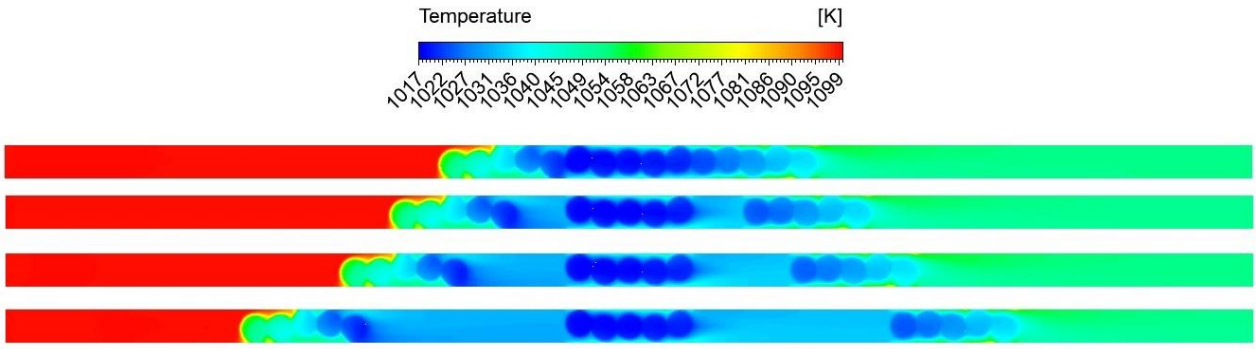

Fig. 20. Temperature contour for catalysts with spherical shape with wall heat flux

Figure 21 and Figure 22 show the dependence of pressure drop for different packing layers along the central cross-section of the reactor tube throughout the tube length. It can be seen that with an increase in X, the pressure drop shifts, while a smooth drop is observed at a distance of X equal to 0 mm.

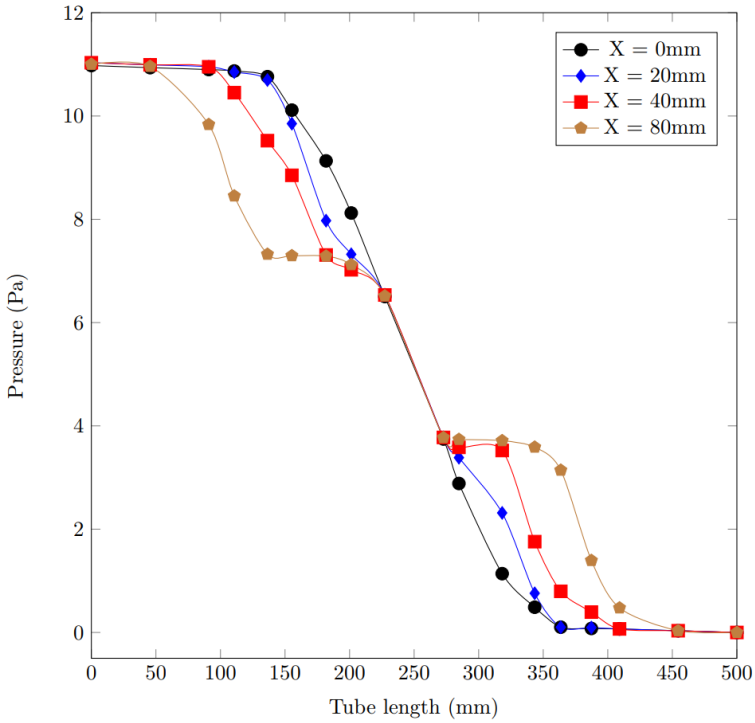

Fig. 21. Pressure drop along the length of the pipe (cylindrical catalysts)

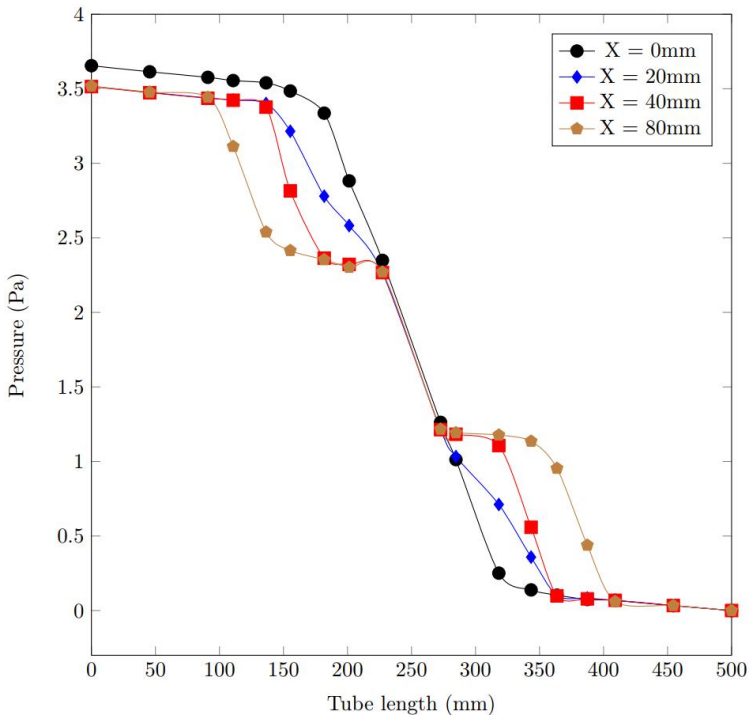

Fig. 22. Pressure drop along the length of the pipe (spherical catalysts)

Figure 23 and Figure 24 show diagrams of the CH_4 and H_2 content for different arrangement of the packing layers. When heat is supplied to the packed bed, an intensification of the steam methane reforming reaction is observed, which is a natural process. It is also seen that hydrogen yield is the highest on the cylindrical shape of the catalysts and the distance between the packing layers equal to 40 mm.

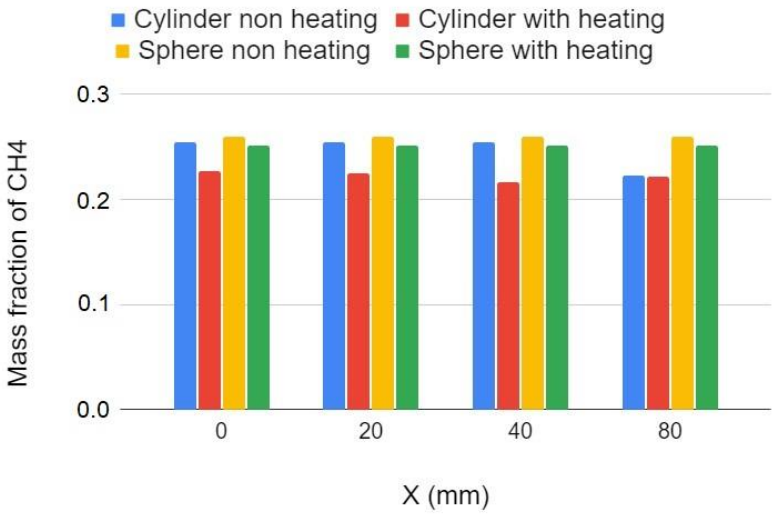

Fig. 23. CH_4 outlet concentration for different arrangement of the packed bed

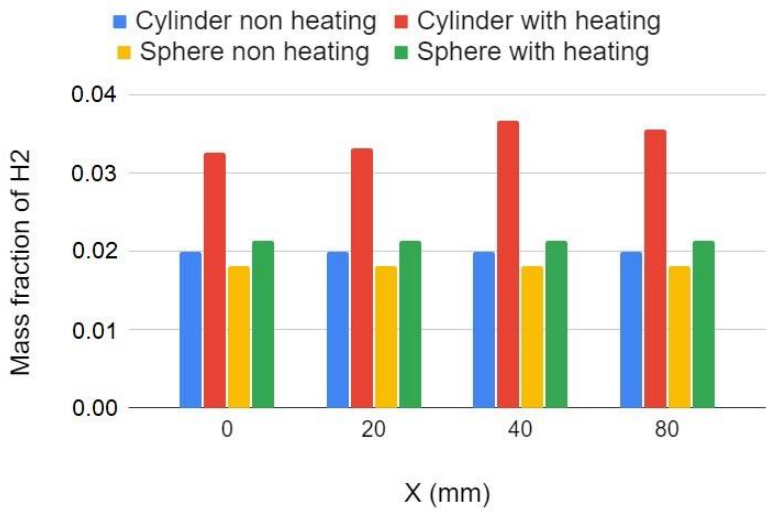

Fig. 24. H_2 outlet concentration for different arrangement of the packed bed

4. Conclusion

The influence of the packed bed arrangement on the reaction process characteristics has been studied in the present article.

If cylindrical catalysts are used and packing sections are placed at different distances from each other, it is possible to intensify the hydrogen output. But with an increase in the distance between the packing layers, the pressure drop shifts, which must be taken into account for the choice of reformer design. The obtained results indicate that the best hydrogen yield is achieved when the distance between packing sections is in the range of 40-80 mm. Intensification of methane conversion occurs only when heat is supplied to the catalyst packing through the reformer wall. With the ability to change the heat supply it is possible to control the operation of the reactor itself, which helps with different operating modes.

If more streamlined forms of catalysts are taken, for example, the spherical shape, then changing the distance between the packing sections will not affect the reforming process. It can be seen from the obtained results that the turbulence of the flow behind the catalysts is too small to give a significant increase in the conversion rate of methane. But at the same time, the location of the packing sections at different distances from each other will allow the reactor to be used in different operating modes.

This study makes a considerable contribution to the reformer design offering a way of increasing steam methane reforming process efficiency. Moreover, that study could be freely used to investigate packed beds with other arrangements and element shapes.

Acknowledgement
This work is supported by the Russian Science Foundation under grant 19-19-00327.

References

[1] Pashchenko, Dmitry. "Thermochemical waste-heat recuperation by steam methane reforming with flue gas addition." *International Journal of Energy Research* 43, no. 6 (2019): 2216-2226. https://doi.org/10.1002/er.4436
[2] Pashchenko, Dmitry. "Experimental study of methane reforming with products of complete methane combustion in a reformer filled with a nickel-based catalyst." *Energy Conversion and Management* 183 (2019): 159-166. https://doi.org/10.1016/j.enconman.2018.12.102
[3] Dixon, Anthony G., Michiel Nijemeisland, and E. Hugh Stitt. "Packed tubular reactor modeling and catalyst design using computational fluid dynamics." *Advances in Chemical Engineering* 31 (2006): 307-389. https://doi.org/10.1016/S0065-2377(06)31005-8
[4] Nijemeisland, Michiel, Anthony G. Dixon, and E. Hugh Stitt. "Catalyst design by CFD for heat transfer and reaction in steam reforming." *Chemical Engineering Science* 59, no. 22-23 (2004): 5185-5191. https://doi.org/10.1016/j.ces.2004.07.088
[5] Konahina, I. A., I. R. Gil'Manshin, and T. R. Safin. "Heightening of efficiency fuel using installations due to external recuperation units of waste heat." *In IOP Conference Series: Materials Science and Engineering* 69, no. 1, p. 012009. IOP Publishing, (2014). https://doi.org/10.1088/1757-899X/69/1/012009
[6] Pashchenko, Dmitry. "Industrial furnaces with thermochemical waste-heat recuperation by coal gasification." *Energy* 221 (2021): 119864. https://doi.org/10.1016/j.energy.2021.119864
[7] Pashchenko, Dmitry, Ravil Mustafin, and Anna Mustafina. "Steam methane reforming in a microchannel reformer: Experiment, CFD-modelling and numerical study." *Energy* 237 (2021): 121624. https://doi.org/10.1016/j.energy.2021.121624
[8] Popov, S. K., I. N. Svistunov, A. B. Garyaev, E. A. Serikov, and E. K. Temyrkanova. "The use of thermochemical recuperation in an industrial plant." *Energy* 127 (2017): 44-51. https://doi.org/10.1016/j.energy.2017.03.091
[9] Pashchenko, Dmitry, Ravil Mustafin, and Anna Mustafina. "Steam methane reforming in a microchannel reformer: Experiment, CFD-modelling and numerical study." *Energy* 237 (2021): 121624. https://doi.org/10.1016/j.energy.2021.121624
[10] Kamarudin, Saddam, Ishkrizat Taib, Nurul Fitriah Nasir, Zainal Ariff Abidin, Hazimuddin Halif, A. M. T. Arifin, and Mohd Noor Abdullah. "Comparison of Heat Propagation Properties in Different Sizes of Malignant Breast Tumours using Computational Fluid Dynamics." *Journal of Advanced Research in Applied Sciences and Engineering Technology* 28, no. 3 (2022): 368-375. https://doi.org/10.37934/araset.28.3.368375
[11] Jamalabadi, Mohammad Yaghoub Abdollahzadeh. "Parameter study of porosity effects on surface temperature for a porous block under wind, water source and thermal radiation." *Journal of Advanced Research in Applied Sciences and Engineering Technology* 29, no. 1 (2022): 295-315. https://doi.org/10.37934/araset.29.1.295315
[12] Pashchenko, Dmitry. "Thermochemical recuperation by ethanol steam reforming: Thermodynamic analysis and heat balance." *International Journal of Hydrogen Energy* 44, no. 59 (2019): 30865-30875. https://doi.org/10.1016/j.ijhydene.2019.10.009
[13] Pashchenko, D. I. "Thermochemical recovery of heat contained in flue gases by means of bioethanol conversion." *Thermal Engineering* 60, no. 6 (2013): 438-443. https://doi.org/10.1134/S0040601513060062
[14] Karthik, G. M., and Vivek V. Buwa. "Effect of particle shape on fluid flow and heat transfer for methane steam reforming reactions in a packed bed." *AIChE Journal* 63, no. 1 (2017): 366-377. https://doi.org/10.1002/aic.15542
[15] Calis, H. P. A., J. P. B. C. Nijenhuis, B. C. Paikert, F. M. Dautzenberg, and C. M. Van Den Bleek. "CFD modelling and experimental validation of pressure drop and flow profile in a novel structured catalytic reactor packing." *Chemical Engineering Science* 56, no. 4 (2001): 1713-1720. https://doi.org/10.1016/S0009-2509(00)00400-0

[16] Menter, Florian R. "Two-equation eddy-viscosity turbulence models for engineering applications." *AIAA journal* 32, no. 8 (1994): 1598-1605. https://doi.org/10.2514/3.12149
[17] Manual, U. D. F. "ANSYS FLUENT 12.0." *Theory Guide* (2009).
[18] Wilke, C. R., and C. Y. Lee. "Estimation of diffusion coefficients for gases and vapors." *Industrial & Engineering Chemistry* 47, no. 6 (1955): 1253-1257. https://doi.org/10.1021/ie50546a056
[19] Fuller, Edward N., Paul D. Schettler, and J. Calvin Giddings. "New method for prediction of binary gas-phase diffusion coefficients." *Industrial & Engineering Chemistry* 58, no. 5 (1966): 18-27. https://doi.org/10.1021/ie50677a007
[20] Hou, Kaihu, and Ronald Hughes. "The kinetics of methane steam reforming over a Ni/α-Al2O catalyst." *Chemical Engineering Journal* 82, no. 1-3 (2001): 311-328. https://doi.org/10.1016/S1385-8947(00)00367-3
[21] Pashchenko, Dmitry, and Anton Eremin. "Heat flow inside a catalyst particle for steam methane reforming: CFD-modeling and analytical solution." *International Journal of Heat and Mass Transfer* 165 (2021): 120617. https://doi.org/10.1016/j.ijheatmasstransfer.2020.120617
[22] Xu, Jianguo, and Gilbert F. Froment. "Methane steam reforming, methanation and water-gas shift: I. Intrinsic kinetics." *AIChE journal* 35, no. 1 (1989): 88-96. https://doi.org/10.1002/aic.690350109
[23] Tacchino, Valeria, Paola Costamagna, Silvia Rosellini, Valter Mantelli, and Alberto Servida. "Multi-scale model of a top-fired steam methane reforming reactor and validation with industrial experimental data." *Chemical Engineering Journal* 428 (2022): 131492. https://doi.org/10.1016/j.cej.2021.131492